Reconstruction of elastic events

J. Kašpar

June 15, 2008

Abstract

This note describes an elastic event reconstruction method developed for the TOTEM experiment. It is based on linear track parameterization and linear track fit. The suggested method has been implemented within simulation/reconstruction software framework and results for 1540 and 90 m optics are given. Obtained resolution is compared to analytic estimates presented in the appendix.

1. Introduction

The step which precedes the elastic reconstruction is fit on one-RP level. The results of that step are local track fits, i.e. positions x, y and angles ϑ_x, ϑ_y (plus covariance matrix for all these parameters). However, one RP (ca 3 cm thick) presents a lever-arm too small for an interesting angular measurement, see Fig. 1. And therefore, only position information can be used for fitting.

In principle, one may also employ the knowledge of vertex distribution at the IP. That can be understood as a fictitious measurement at IP with uncertainty given by beam width. Corresponding optical functions would be $L = 0$ m, $v = 0$ for both projections. The question whether this makes sense will be addressed after presenting the method and the algorithm of reconstruction.

Regardless whether the IP information is used, input data form a list of $(x, \sigma_x, y, \sigma_y | L_x, L_y, v_x, v_y)$, one per RP (or IP measurement).

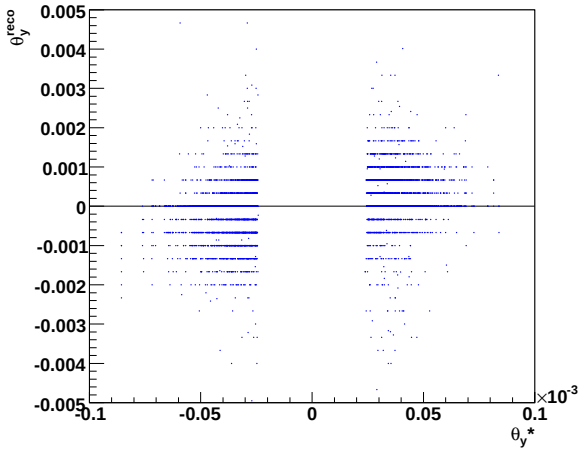

Figure 1: ϑ_y generated (at IP) vs. reconstructed (at RP) for 90 m optics: no interesting correlation. The reason is too small lever-arm for the given detector pitch. One can clearly see the strip pattern.

2. Method

Tracks of protons travelling from IP to detectors can be well described by [1)]

$$x(s) = L_x(s)\,\vartheta_x^* + v_x(s)\,x^* + D(s)\,\xi \qquad y(s) = L_y(s)\,\vartheta_y^* + v_y(s)\,y^*\,, \tag{1}$$

[1)] We use the standard coordinate frame: s axis goes along beam in clock-wise direction and x points outside the ring. y axis is chosen such as the coordinate system is right-handed.

where the quantities with stars refer to the state of the proton at IP. For elastic scattering $\xi \equiv 0$ and therefore dependencies for both coordinates obtain the same form. Thus, ζ will be used to refer to whichever of x and y variables.

Obviously, the fitting model used is

$$\zeta(s) = v(s)\,\zeta^* + L(s)\,\vartheta^* \,. \tag{2}$$

Working out the linear fit equations (see e.g. Eq. (6.23) in [1]), the estimate for vertex position ζ^* and scattering angle (at vertex) ϑ^* is

$$\begin{pmatrix} \zeta^* \\ \vartheta^* \end{pmatrix} = \frac{1}{\sum v^2 \sum L^2 - \sum vL \sum vL} \begin{pmatrix} \sum L^2 \sum \zeta v - \sum vL \sum \zeta L \\ -\sum vL \sum \zeta v + \sum v^2 \sum \zeta L \end{pmatrix} , \tag{3}$$

where for instance $\sum \zeta L$ means $\sum_i \zeta(s_i) L(s_i)/\sigma^2(s_i)$. The sums go over all detectors involved in the event and $\zeta(s_i)$ is the hit position in corresponding detector. σ denotes measurement uncertainty. The covariance matrix (see e.g. Eq. (6.24) in [1])

$$\mathrm{Var}[\zeta^*, \vartheta^*] = \frac{1}{\sum v^2 \sum L^2 - \sum vL \sum vL} \begin{pmatrix} \sum L^2 & -\sum vL \\ -\sum vL & \sum v^2 \end{pmatrix} . \tag{4}$$

3. Algorithm

The algorithm comprises the three steps below.

1) *Hit selection*. The aim of this step is to choose from all the hits only those which belong to the actual track (of elastic protons). Which in turn means to suppress background and tracks from secondary interactions in detectors etc. It is assumed that the $L\,\vartheta^*$ term dominates in Eq. (2), i.e. at least approximate parallel-to-point focusing. For each hit, value of $\zeta(s)/L(s)$ is calculated and a road search algorithm is applied. Only road with the highest weight and at least one hit on both sides can continue. Parameters of this search are (angular) road sizes for x and y projections.

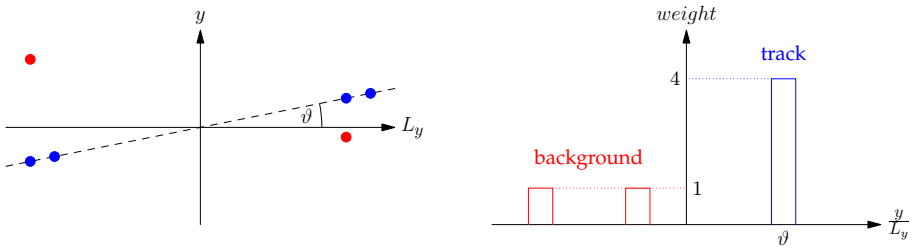

Figure 2: Principle of the road search algorithm. Left: hits in RPs shown vs. corresponding effective length. Hits by elastic protons displayed in blue, background in red. Right: histogram of angles y/L_y. Elastic hits pile up to high tower (i.e. road with highest weight).

2) *Fitting*. There are three fits performed: left-arm fit, right-arm fit and global fit. Obviously, left-arm fit is carried out through hits from the left-arm only (plus IP if applicable), etc.

3) *Cut application*. This step is used to distinguish elastic scattering from other processes. It exploits properties of elastic scattering, namely reconstructed angles and vertex positions shall be identical for left and right fits. Therefore, the cut requires the left-right differences to be smaller than a certain limit. The parameters of this step are, hence, angular and vertex difference tolerances. Indeed, for both projections x and y.

4. Usefulness of IP information

Here, we are coming back to the question whether it is worth adding a fictitious measurement at IP to the list of hits [2]. To answer the question, let's assume the optics is symmetric i.e.

$$L(-s) = -L(s), \qquad v(-s) = v(s)$$

(that assumption is true for ideal 1540 and 90 m optics). Then [3], the fit equation boils down to

$$\zeta^* = \frac{\sum \zeta v}{\sum v^2}, \qquad \vartheta^* = \frac{\sum \zeta L}{\sum L^2}\,. \tag{5}$$

One can clearly see that the IP measurement has no impact on angular reconstruction of ϑ^*. As effective length associated to IP is zero, both numerator and denominator remain unchanged. The situation is different for ζ^* reconstruction, so let's rewrite the expression explicitly separating RP and IP contributions

$$\zeta^* = \frac{\sum \frac{\zeta_i v_i}{\sigma_i^2} + \frac{\zeta_{\mathrm{IP}}}{\sigma_{\mathrm{IP}}^2}}{\sum \frac{v_i^2}{\sigma_i^2} + \frac{1}{\sigma_{\mathrm{IP}}^2}}\,,$$

where the index $i = 1 \ldots N$ labels RP hits. Looking at denominator, one can estimate that the influence of IP information would be irrelevant if

$$v \gg \frac{1}{\sqrt{N}}\,\frac{\sigma}{\sigma_{\mathrm{IP}}}\,, \tag{6}$$

where v denotes a typical value of v_i and similarly σ means typical σ_i. Validity of this condition can verified with use of Tabs. 1 and 2. For 1540 m optics one finds both sides of Eq. (6) to be of order 10^{-2} and thus the condition is false. While for 90 m optics the condition $2 \gg 6 \cdot 10^{-2}$ is true. Anyway, vertex reconstruction is not our primary concern and therefore IP information will not be used unless necessary.

The necessity for IP information may be seen in the following example. Imagine the situation where only one RP per arm was active in the event. We need to perform one-arm fits to verify the identity of the event, but one hit is not enough to fit two parameters. This is the only case when the IP information is used.

5. Estimate of the parameters

As explained above, there are 6 parameters governing the reconstruction, namely road sizes, angular and vertex tolerances for both projections. Here, we try to estimate reasonable values of those parameters.

The road size is meant as a coarse seed for principal track search. Thus, it makes sense to set it to approximately to T/L, where T is size of a trigger zone and L is typical effective length. The road size should definitely distinguish between top and bottom RPs. That is if Δ is distance between top and bottom RP edges, the road size should be $< \Delta/L$.

Regarding the angular tolerance parameter, a good choice seems to be a few times pitch/L, where again L is a typical effective length. However, in the case when beam divergence is present, the tolerance should become $\approx \sigma(\text{beam divergence})$.

Having in mind the 90 and 1540 m optics, it is difficult to make any estimate for vertex tolerance. The problem arises from very small magnifications v. However, it is easy to simulate elastic events only, apply the reconstruction with no cuts and make histograms of left-right fit differences. Eventually, the tolerance parameters can be deduced from those histograms.

[2] Let us remark that IP information has a different statistical nature than RP measurement. Let's have a particle passing through a RP at position ζ. Due to measurement errors the detector reports the particle at position ζ_m. In the language of statistics, ζ_m is a sample of some distribution D, which reflects properties of measurement errors. It is reasonable to assume that mean value of D is ζ, i.e. the actual particle position. Regarding the IP information, the role of mean and actual position is swapped. We put the fictitious measurement to $\zeta = 0$ (vertex mean) while the real vertex position is unknown. A naive mixing RP and IP information may, therefore, lead to inconsistencies. Nevertheless, both types of informations can be safely used withing LS method since the method is only sensitive to distance between actual and mean position.

[3] In fact, one has to assume the fit to be symmetric too. That means if a RP at s was hit, its partner at $-s$ was involved too. However, this should be true for most events.

6. Performance at $\beta^* = 1540$ m optics

The reconstruction method was probed on a sample of 10^4 elastic events, generated in t-range 10^{-3} GeV^2 to 1.5 GeV^2. The actual parameters of optics and detector geometry are summarized in Tab. 1. The simulation was carried out first without beam smearing and then including it (see the next two subsections). The beam smearing characteristics can be found in Tab. 2.

The road size parameters were set to 5 μrad for x (the Δ/L estimate) and 8 μrad for y coordinate (the T/L estimate, $T = 32 \cdot 66$ μm). The tolerance parameters were set to huge numbers so no cuts were applied.

Let us recall that double arm fits were employed (details in section 3) and no vertex information used (more in section 4).

β^* (m)	ε (μm $\cdot$ rad)	L_x (m)	v_x	L_y (m)	v_y	δ_x (mm)	δ_y (mm)
1540	1	110	$6 \cdot 10^{-2}$	270	$2 \cdot 10^{-2}$	0.80	1.35
90	3.75	2.9	2.2	265	$2 \cdot 10^{-2}$	4.15	6.40

Table 1: Description of optics and detector geometry for station at 220 m. ε stands for emittance. L_x, v_x, L_y and v_y represent typical values of the optical functions. Here, we put their maximal values as those contribute most to the fit. And δ_x or δ_y denotes distance between beam and edge of horizontal or vertical detector.

β^* (m)	σ_ϑ (μrad)	σ_v (μm)	σ_ξ	crossing angle (rad)
1540	0.295	321	10^{-4}	0
90	2.4	150	10^{-4}	0

Table 2: Smearing parameters used for simulation. σ_ϑ denotes sigma of beam divergence, σ_v spread of vertex distribution and σ_ξ variance of energy smearing. Full explanation of smearing simulation and its parameters is to be found at [2].

6.1. Case without beam smearing

Fig. 3 shows errors of angular and vertex reconstruction. The right plot clearly demonstrates that vertex resolution is poor for this optics. Relative error of t determination is shown in Fig. 4. The blue curve represents fit of $A/\sqrt{t}$ and it describes the data well. The fit gives $A = 0.9 \cdot 10^{-3}$ GeV, while the estimate Eq. (A.13) predicts $A = 0.8 \cdot 10^{-3}$ GeV (for $N = 6$). One can conclude that both values well agree.

Figs. 5 and 6 demonstrate statistical behavior of the fits. One should emphasize that uncertainty of RP spatial measurement was fixed to 66 μm$/\sqrt{12}$ [4]. Majority of events produced fits with two and four degrees of freedom, that means 4 and 6 RPs were hit. The most frequent hit configuration includes 2 vertical RPs at each side and 2 horizontal RPs at one side. The second most frequent case comprises only 2 vertical RPs at each side. Fig. 6 shows distributions of normalized residual sums for theses two dominant hit configurations. The red and blue curves represent theoretical χ^2 distributions. There is an evident small discrepancy, the residual sums seems to be squeezed to smaller values. This suggests that measurement uncertainties were overestimated. The right-hand side plot of Fig. 5 shows a histogram of reconstruction error divided by fit uncertainty for ϑ_y. Ideally, it should be a Gaussian with unit variance. The variance obtained is just slightly higher.

[4] In fact, as there are 5 planes for each coordinate, one might expect resolution of 66 μm$/\sqrt{12 \cdot 5}$. However, it is a profound fact that a vast majority of protons hit all the five detector planes within the same strip. That's why one cannot directly apply the $1/\sqrt{N}$ statistical rule.

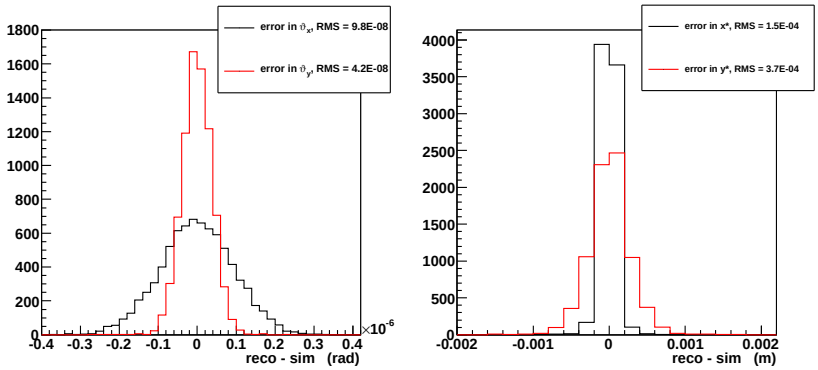

Figure 3: Angular (left) and vertex (right) resolutions.

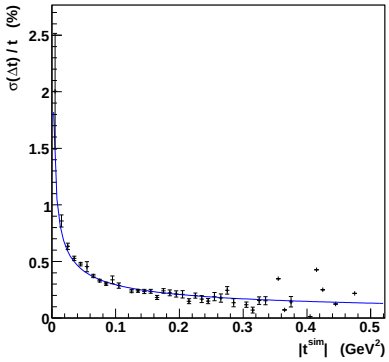

Figure 4: Relative t resolution.

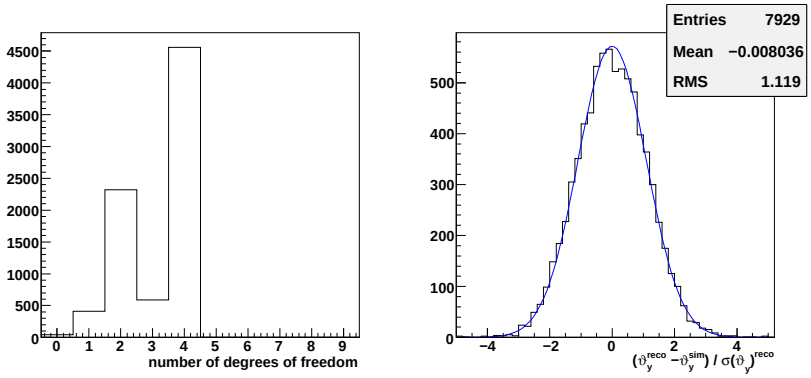

Figure 5: Left: histogram of numbers of degrees of freedom. Right: ϑ_y reconstruction error divided by fit uncertainty (blue line represents a Gaussian fit).

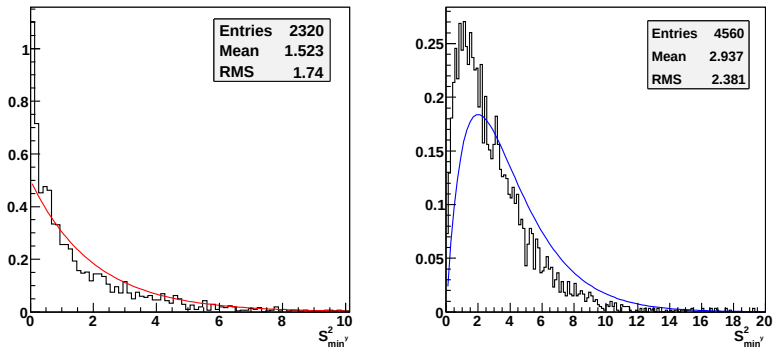

Figure 6: Histograms of normalized residual sums (for y fits, plots for x fits look similarly). Left for 2 degrees of freedom, right for 4. Red and blue curves show theoretical χ^2 distributions.

Before moving to the next section, let's briefly discus efficiency of the algorithm, i.e. numbers of rejected events. The results are shown in Tab. 3. One can see quite low number ($< 2\%$) of inconsistent fits, which is correct as no constraints were imposed. The present number corresponds to pathological events (e.g. when a proton interacts in front RP and therefore measurement in back RP is misleading). There are many events empty or insufficient. However, this can be easily explained geometrically. Assuming that t distribution falls off exponentially, i.e. $t \sim b\exp(-bt)$, and φ is uniformly distributed on $\langle 0, 2\pi)$, one finds that angles ϑ_x and ϑ_y are independent and follow normal distribution $N(0, \sigma^2 = 1/2bp^2)$ where p is momentum of protons. Therefore, probability of $|\vartheta_y| < \vartheta_y^{\min}$ is given by

$$P(|\vartheta_y| < \vartheta_y^{\min}) = \mathrm{Erf}(\vartheta_{\mathrm{y}}^{\min}/\sqrt{2\sigma^2}) \,. \tag{7}$$

And consequently, fraction of empty and insufficient events is

$$P(\text{empty}) = \mathrm{Erf}\left(\frac{\delta_y\, p\,\sqrt{b}}{L_y}\right)\,\mathrm{Erf}\left(\frac{\delta_x\, p\,\sqrt{b}}{L_x}\right) \approx 4.4\,\% \,, \tag{8}$$

$$P(\text{insufficient}) = \mathrm{Erf}\left(\frac{\delta_y\, p\,\sqrt{b}}{L_y}\right)\,\left[1 - \mathrm{Erf}\left(\frac{\delta_x\, p\,\sqrt{b}}{L_x}\right)\right] \approx 13\,\% \,, \tag{9}$$

where $b \approx 20$ GeV^{-2} was used and δ and L parameters are to be found in Tab. 1. These estimates correspond well with Tab. 3 (one should keep in mind that many effects, like insensitive edge, were not taken into account).

	fully reconstructed	empty events	insufficient events	inconsistent x^*	inconsistent y^*	inconsistent ϑ_x	inconsistent ϑ_y
without smearing	7867	426	1557	0	8	125	17
with smearing	7801	414	1548	0	5	154	78

Table 3: Efficiency of the algorithm (sample of 10^4 events). Column "empty events" refers to events with no signal and column "insufficient events" with signal insufficient to perform the fit (see step 1 in the algorithm, section 3). The four right-most columns show numbers of events rejected because of inconsistent right and left fits (see step 3 of the algorithm).

6.2. Case with beam smearing

Fig. 7 shows precision of angular and vertex reconstruction. The dominant error source for angular reconstruction is the beam divergence and therefore all ϑ_x, ϑ_y and ϑ variances are practically identical [5)]. The relative t-resolution shown in Fig. 8 was fitted by $A/\sqrt{t}$ (as suggested by Eq. (A.14)) yielding $A = 2.2 \cdot 10^{-3}$ GeV. Analytical estimate gives $A = 2.2 \cdot 10^{-3}$ GeV, which agrees with fit result.

As already said, it is useful to plot right-left fit differences, see Fig. 9. This information can be used to set reasonable values of tolerance parameters (of course, these plots should be compared to corresponding plots obtained for background). Considering the properties of the optics (parallel-to-point focusing), one can expect rather a wide distribution of vertex differences. This expectation is well supported by the figure. Therefore, cut based on vertex differences is not very promising. Regarding $\Delta_{R-L}\vartheta_y$, it is reasonable to expect it to be dominated by beam divergence. In other words, its distribution shall have RMS of beam divergence (compare Eqs. (A.3) and (A.4)). It really does, but one might be surprised by the peaks.

[5)] Since $\vartheta^2 = \vartheta_x^2 + \vartheta_y^2$ one may naively expect that $\sigma_\vartheta > \sigma_{\vartheta_{x,y}}$. However, a careful error propagation yields

$$\sigma_\vartheta^2 = \sigma^2\left(\sqrt{\vartheta_x^2 + \vartheta_y^2}\right) = \frac{\vartheta_x^2}{\vartheta_x^2 + \vartheta_y^2}\,\sigma_{\vartheta_x}^2 + \frac{\vartheta_y^2}{\vartheta_x^2 + \vartheta_y^2}\,\sigma_{\vartheta_y}^2 = \frac{\sigma_{\mathrm{bd}}^2}{2} \,.$$

In the last step we employed $\sigma_{\vartheta_x} = \sigma_{\vartheta_y} = \sigma_{\mathrm{bd}}/2$ (compare with $\delta\vartheta_x$ in Eq. (A.4)). Therefore variances of ϑ, ϑ_x and ϑ_y are equal.

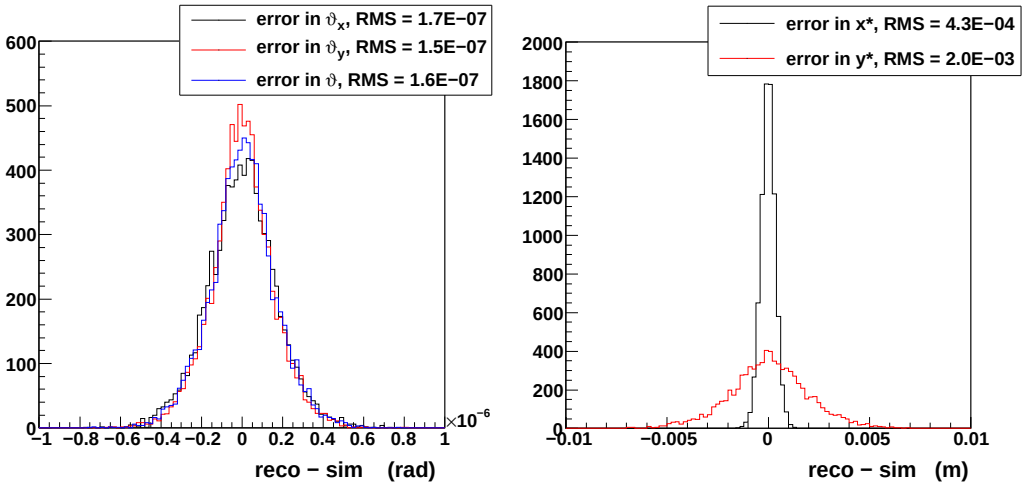

Figure 7: Angular (left) and vertex (right) resolutions.

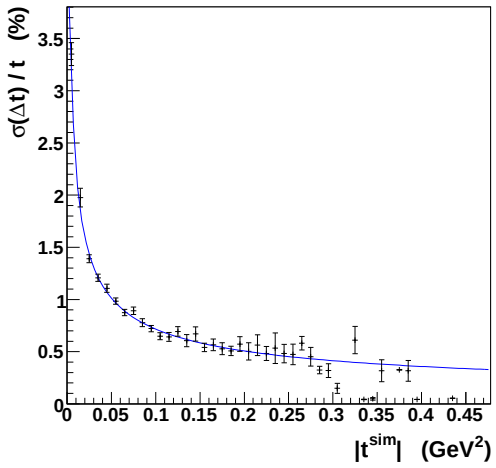

Figure 8: Relative t resolution.

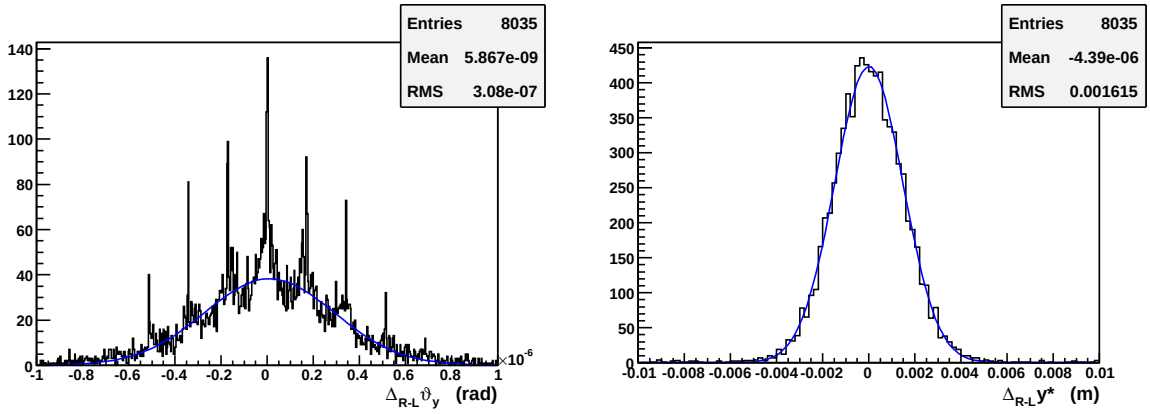

Figure 9: Right-left differences in ϑy and y^* fit results. Plots for x coordinate are qualitatively the same.

To understand the peak appearance, we should go back and discuss what data are inserted to the reconstruction algorithm. Every RP has 5 u and 5 v strip detectors. Measurements from each group are (roughly speaking) averaged, yielding one u, v point per RP. This point is, then, rotated by 45 ° to obtain x and y coordinates of the hit. The detectors have strip pitch $P = 66$ μm and therefore any possible (single detector) measurement outcome can be written as

$$u \text{ or } v = \text{const.} + P\,k\ , \tag{10}$$

where k is an integer. Moreover, particles detected in RPs have very small scattering angles and thus, very often, the same strip is hit in all 5 u, resp. v strip detectors. This means that the averaged u, v coordinates are peaked at values given by Eq. (10). After the rotation to x, y space, the peaks in hit distribution are separated by $P/\sqrt{2}$ (this is the gap between two closest x or y outcomes). This fact is documented by Fig. 10A.

Now, one may insert Eq. (10) to Eq. (3) and find where the peaks of angular distributions are. However, performing that in full generality would be complicated and not instructive. But, let's try out the (so far well working) approximation from Appendix A. Inserting $y_i = y_i^0 + k_i P/\sqrt{2}$ into Eq. (A.1) yields

$$\vartheta_y' = \vartheta_y^0 + \frac{P}{NL_y\sqrt{2}} \left(\sum_R k_i - \sum_L k_i \right) . \tag{11}$$

Since the factor in parentheses is integer, peaks at distance $P/(\sqrt{2}NL_y)$ can be expected. Using this equation, let's express the right-left difference

$$\Delta_{R-L}\vartheta_y \equiv \vartheta_y^R - \vartheta_y^L = \text{const.} + \frac{P}{2L_y\sqrt{2}} \left(\sum_R k_i + \sum_L k_i \right) = \text{const.} + \frac{P}{L_y\sqrt{2}}(k^R + k^L) , \tag{12}$$

where, for simplicity, we constrained ourselves to the case with 2 hits per arm. In this simple approach, all effective L are identical within one arm and therefore so k_i's are. In other words $\sum_R k_i = 2k^R$, which justifies the last equality in Eq. (12). The peaks are predicted with spacing $P/(\sqrt{2}L_y) \approx 0.17\,\text{rad}$, which perfectly agrees with Fig. 9.

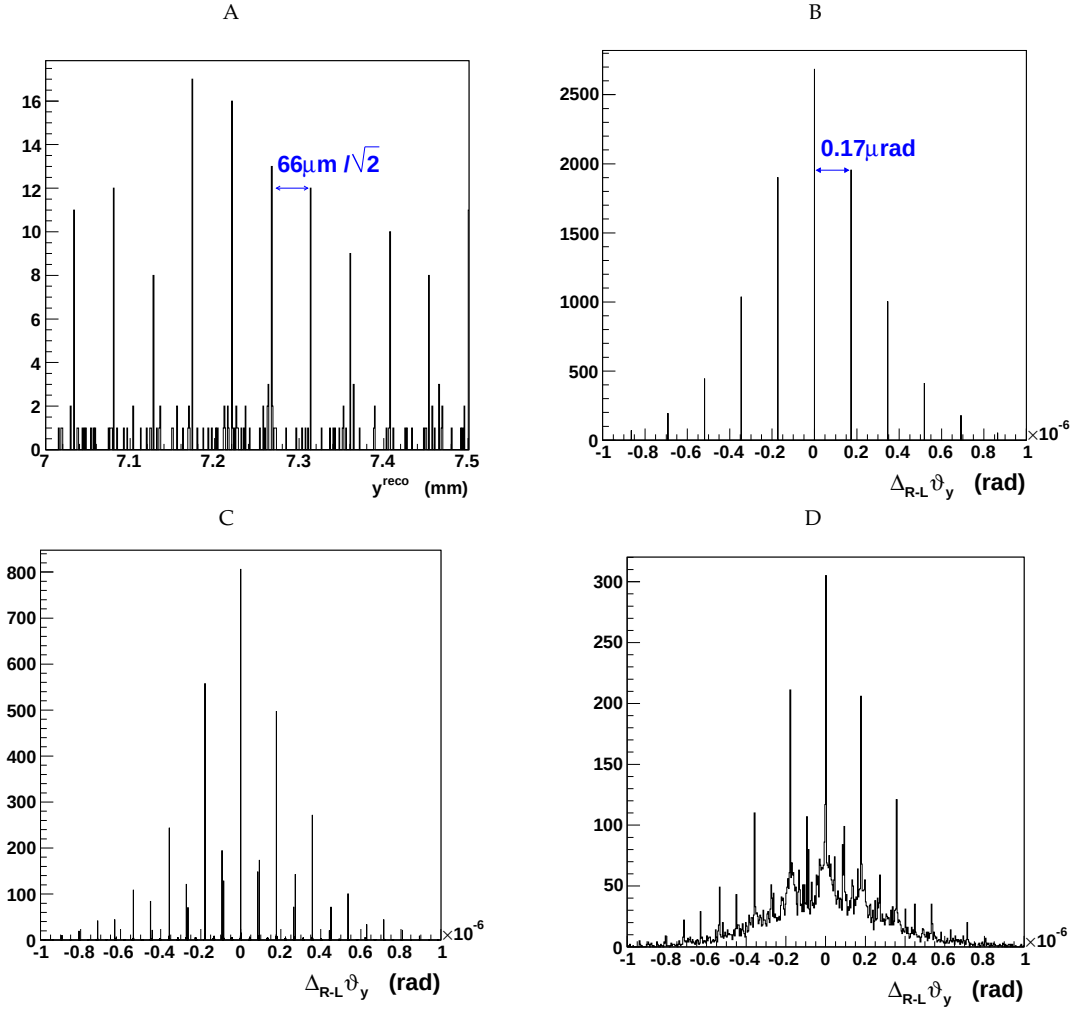

Figure 10: To the explanation of peaks in ϑ_y distribution. Plot A shows quantization of measured y coordinate. The other three plots describe steps of MC simulation: single effective length approach (B), realistic effective length used (C) and finally partial (strip-)quantization included (D).

There have been two important facts omitted in the previous paragraph: different effective lengths present and several hits counts (e.g. the dominant configuration has 4 hits at one arm and 2 at the other). It would be complicated to incorporate those two effects in the analytic calculation and that is why we rather performed a simple MC simulation. The results are shown in Fig. 10. Plot A corresponds to the approximation of the previous paragraph. Plot B was obtained for realistic L_i values and for $2+2$ and $4+2$ hit configurations. Eventually, we added the effect of partial (strip-)discretization of y values and the plot C was obtained. This plot well reproduces Fig. 9. However, note the secondary structure with half pitch of the main peaks in the MC plot. This is probably due to other effects not included to the MC simulation.

As the last comment, let's address the detector shifts. Displacing horizontal detectors would change only the constant terms in Eqs. (10) and (12) and thus the entire peak structure would just move. The same effect takes place if top and bottom vertical pots are shifted simultaneously. But if they are moved independently, the whole picture changes. We stop this discussion here as it is not the primary goal of this article.

7. Performance at $\beta^* = 90$ m optics

Relevant parameters of this optics are summarized in Tab. 1. Immediately, one can see this optics has very low effective lengths L_x, which requires a special treatment. First, the selection algorithm is not intended for such a case and therefore the x road size should be set to a large number in order to let everything pass (the two dimensional road search is, then, reduced to one dimension). Similarly, this is the reason for bad ϑ_x reconstruction performance. Thus no constraints should be imposed on ϑ_x (this is equivalent to very large tolerance parameter).

As for 1540 m optics, we generated 10^4 elastic events ($2.5 \cdot 10^{-2}$ GeV$^2 < |t| < 1.5$ GeV^2), with and without smearing. The y road size was fixed at 50 μrad (the Δ/L estimate) and no vertex cuts (high vertex tolerances) were used for both cases.

7.1. Case without beam smearing

The last parameter which has not been discussed yet, is ϑ_y tolerance. For this section it was set to $6 \cdot 10^{-7}$. It is a very liberal cut which removes only pathological events.

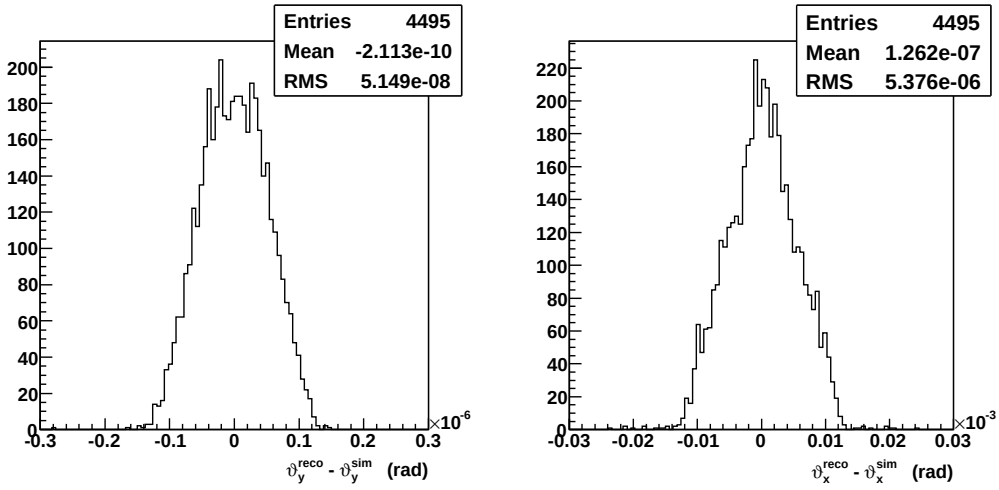

Figure 11: Angular resolution for 90 m optics without smearing.

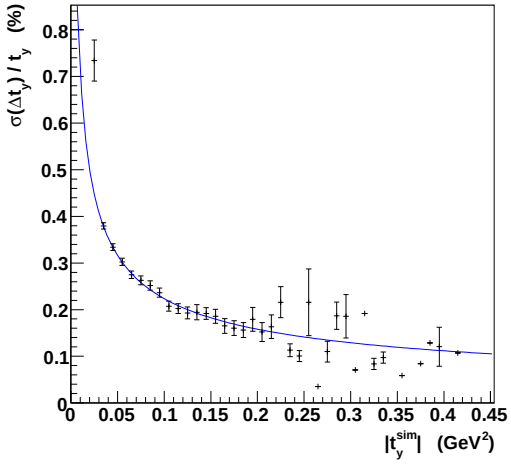

Figure 12: Relative t resolution.

The angular resolution is shown in Fig. 11. The ϑ_x precision is very bad, as expected. Relative error of t_y reconstruction, shown in Fig. 12, was fitted by Eq. (A.13). The fit gives $A = 7.1 \cdot 10^{-4}$ GeV, while analytic estimation yields $A = 5.3 \cdot 10^{-4}$ GeV for $N = 4$, which is the dominant configuration. The analytical uncertainty is apparently slightly underestimated.

Fig. 13 shows vertex reconstruction potential. As magnifications v_y are low for this optics, precision of y^* reconstruction is poor.

Important statistical properties of the fits can be seen in Fig. 14. The left-hand side plot shows that most events include 4 hits, i.e. 2 degrees of freedom. The right-hand plot shows residual sum of squares for events with 2 degrees of freedom. The histogram is compared to $\chi^2(\nu = 2)$ distribution drawn in red. The histogram is quite close to the desired distribution. Fig. 15 presents a histogram of ϑ_y error divided by fit uncertainty. Ideally (if included error sources were Gaussian-like), the histogram should form a Gaussian with RMS one. But since strip-rounding error behaves rather like δx in Eq. (A.4), one need not be surprised that the histogram deviates from Gaussian shape.

Tab. 4 summarizes numbers of rejected events. There is evidently high number of empty events. But again, this can be explained geometrically. In principle, one might follow the same prescription as for 1540 m optics. However, here one should consider relatively high lower bound of simulated events: $2.5 \cdot 10^{-2} < |t|$. Then, the calculation gets complicated. We performed a MC simulation instead, yielding 53 % probability of empty event. This corresponds well to the observed frequencies. As $L_x \approx 0$, horizontal RPs are not involved in elastic events and there is no geometrical reason for insufficient events. Those 103 events correspond to problematic events, for instance when proton was registered at one arm only etc.

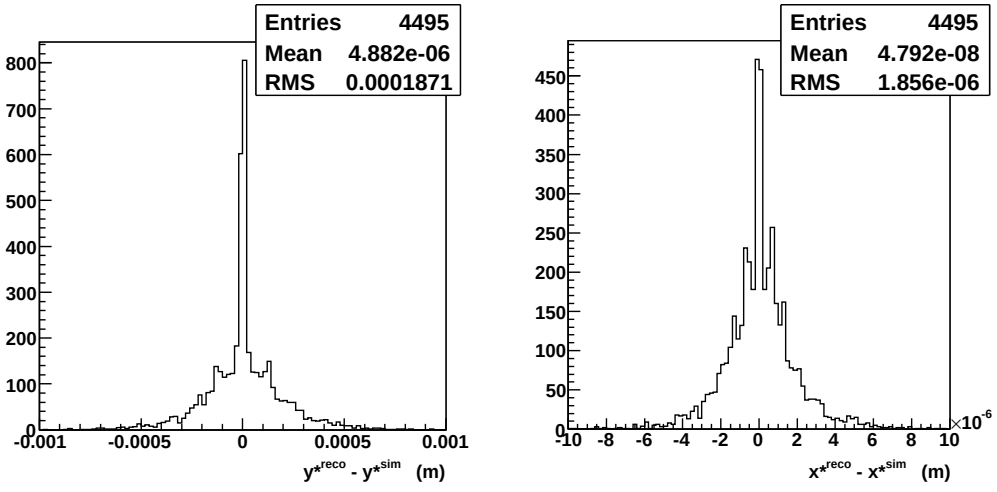

Figure 13: Vertex resolution.

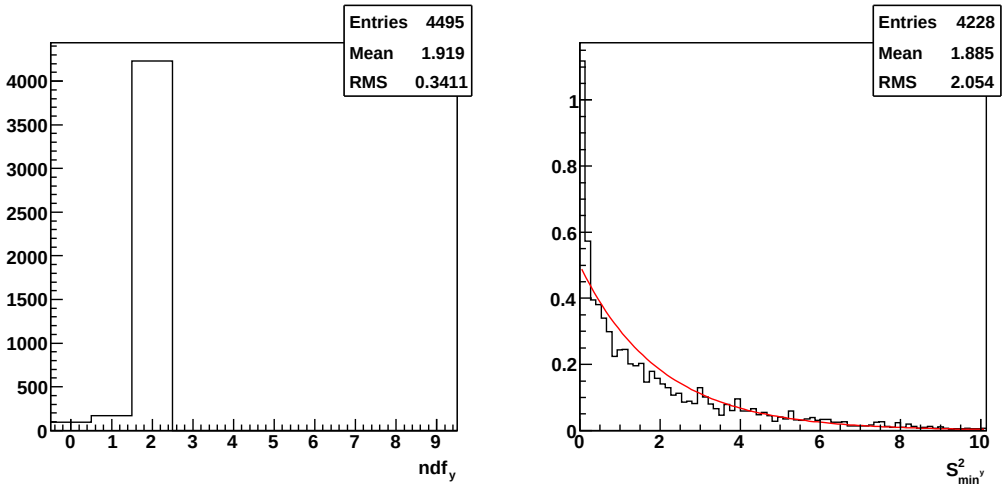

Figure 14: Some statistical properties of the y fit. Left: number of degrees of freedom distribution. Right: Histogram of normalized residual sums for events with 2 degrees of freedom. Red curve represents theoretical χ^2 distribution.

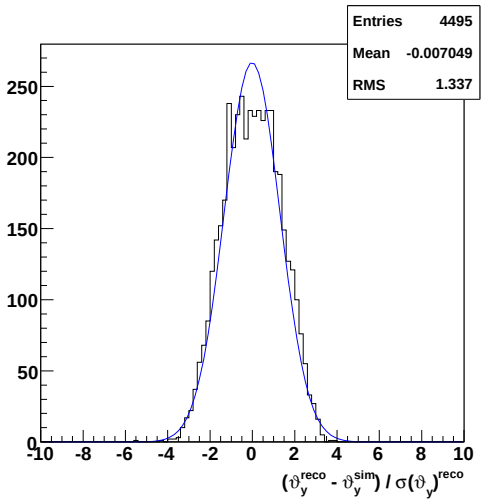

Figure 15: Histogram of ϑ_y deviation divided by fit uncertainty.

	fully reconstructed	empty events	insufficient events	inconsistent x^*	y^*	ϑ_x	ϑ_y
without smearing	4495	5350	103	0	0	0	52
with smearing	4228	5120	605	0	9	0	38

Table 4: Efficiency of the algorithm (sample of 10^4 events). For legend see Tab. 3.

7.2. Case with beam smearing

The analysis was repeated for simulation with smearing applied (smearing parameters are to be found in Tab. 2). The ϑ_y tolerance had to be increased because of the beam divergence. The value used was $8 \cdot 10^{-6}$ rad (compare with left plot of Fig. 18).

Interesting angular and vertex reconstruction results are shown in Fig. 16. Relative errors of t components are plotted in Fig. 17. All of them follow the $A/\sqrt{t_y}$ rule. But as t_x measurement introduces a significant error, only t_y is of practical use. The of t_y resolution gives $A = 1.7 \cdot 10^{-2}$, just as estimate by Eq. (A.13).

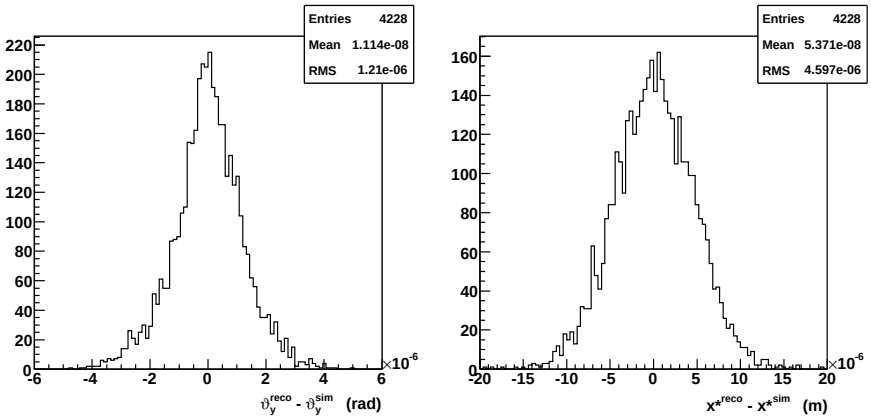

Figure 16: Angular and vertex resolution for 90 m optics with smearing.

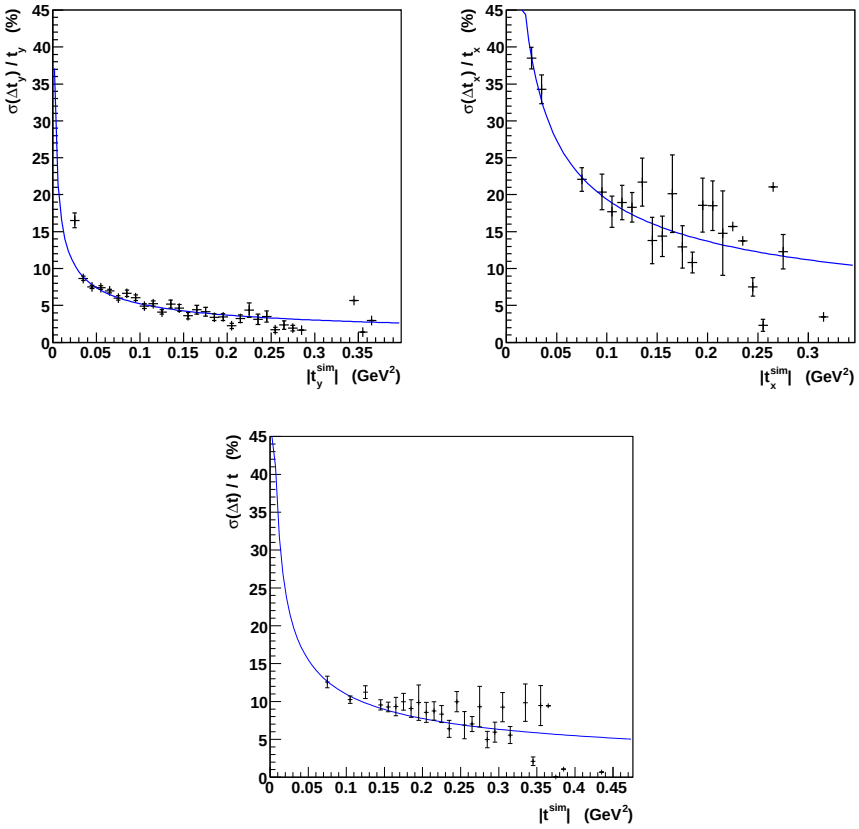

Figure 17: Relative errors of t_y, t_x and t reconstruction.

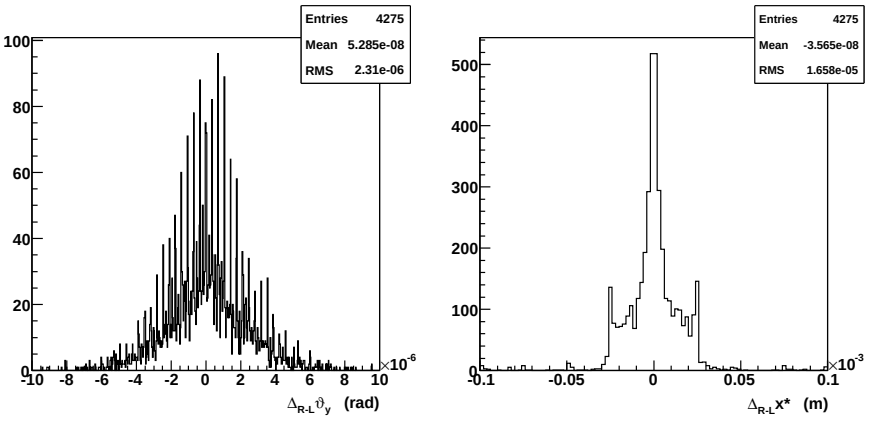

Figure 18: Right-left differences in ϑy and x^* fits.

Finally, right-left difference plots are shown in Fig. 18. The sigma of ϑ_y difference histogram well corresponds to beam divergence variance. Also the peaks are present. We carried out a MC simulation like for the previous optics, but this time the outcome did not fit that well to the data. The major peaks in the simulation are twice closer than the major peaks in data. In fact, this observation is similar to the case of $1540\ \mathrm{m}$ optics. The peaks with half pitch were also present (see Fig. 10D) but were suppressed in comparison with the principal peaks. The reason is, probably, the simple MC is missing some relevant effects and subtleties (which can have only smearing impact).

Looking at Tab. 4 one can see that number of insufficient events rose drastically after inclusion of smearing effects. Those events take place mainly in the region of detector edges and hence it suggest a straight-forward explanation: outgoing protons have slightly different direction due to the beam divergence and it happens that only one proton hits detectors.

8. Discussion

It would be definitely worth testing the performance of the algorithm on a sample of background or background plus elastic events. Unfortunately, only one-arm background simulations are currently available. No surprise that all those events are rejected.

There is one issue already known. Let's imagine a situation when a proton interacts in/after $214\ \mathrm{m}$ unit. Indeed, it gets deflected and if it reaches further detectors, the information is misleading. In such a case one should omit information from affected RPs. That should be done on the level of selection, but unfortunately the present road search algorithm is not sensitive enough. Fortunately, those events are rather rare.

Appendix A. Estimation of t measurement error

In order to cross-check performance of the reconstruction method, it is desirable to estimate reconstruction error. In this appendix, I will express contribution of two main error sources, i.e. beam divergence and finite pitch of detectors.

To keep the calculation smooth, I adopted the assumptions below. Many of those are not precisely fulfilled, but the error caused by them is not dramatic for the purpose of error estimate.

1) The optics is symmetric, therefore the v-terms in track parameterization (see Eq. (2)) cancel out.
2) Absolute values of $|L_x|$ for all RPs do not differ drastically [6)] and can be well approximated by $\pm L_x$. The $+$ sign holds for RPs at right arm and vice versa. The same assumption for L_y.
3) Uncertainties in hit position measurements are identical for all RPs.
4) There are N measurements in total, $N/2$ for each arm.

Under these assumptions, the fit equation (Eq. (3)) can be simplified to

$$\vartheta'_x = \frac{1}{N\,L_x}\left(\sum_{\mathrm{right}} x_i - \sum_{\mathrm{left}} x_i\right)\ . \tag{A.1}$$

From now on, symbols with prime will be related to measured values while prime-less symbols will refer to the true or unsmeared value.

If there were no errors and smearings, x_i would be given by parameterization Eq. (2). But as those are present, one needs to generalize the dependence. Since we assume symmetric optics, we may drop out the v-term and write down

$$x_i = L_x \vartheta_x^{\mathrm{smeared}} + \Delta x_i\ . \tag{A.2}$$

We replaced ϑ_x by its smeared value and added a term which describes discretization to the given pitch. It is natural to assume that Δx_i follows uniform distribution $U(-P/2, P/2)$, where P stands for the

[6)] For instance, for $1540\ \mathrm{m}$ optics L_x ranges from 99 to 113 m and L_y from 248 to 272 m. Therefore, the approximation of unique effective length brings error of roughly 10 %.

detector pitch. For completeness, $\sigma_{\Delta x} = P/\sqrt{12}$. Later on, we will also assume Δx_i to be independent for different RPs.

In note [2] an analysis of angular smearing has been carried out for particles scattered to small angles (i.e. particles that can be detected by Roman Pots). It shows that the effect of smearing is equivalent to modification of particles' direction (see Eq. (16) in [2])

$$\begin{aligned} \vartheta_x \equiv \vartheta\cos\varphi &\to \vartheta\cos\varphi + \Delta\vartheta_x^{L,R} \\ \vartheta_y \equiv \vartheta\sin\varphi &\to \vartheta\sin\varphi + \Delta\vartheta_y^{L,R} \end{aligned} \quad , \tag{A.3}$$

where the standard notation is followed: ϑ denotes scattering angle and φ is azimuthal angle. By the L, R superscript we want to emphasize that the shift has different values for particles at left and right arm.

Inserting Eqs. (A.2) and (A.3) to Eq. (A.1) yields

$$\vartheta'_x = \vartheta_x + \delta\vartheta_x + \frac{1}{L_x}\delta x, \qquad \delta\vartheta_x = \frac{\Delta\vartheta_x^R + \Delta\vartheta_x^L}{2}, \qquad \delta x = \frac{1}{N}\left(\sum_{\text{right}}^{N/2}\Delta x_i - \sum_{\text{left}}^{N/2}\Delta x_i\right) \tag{A.4}$$

Clearly, mean values of both $\delta\vartheta_x$ and δx are zero. Following Eq. (17) [7] in [2] one obtains $\sigma_{\delta\vartheta_x} = \sigma_\vartheta/2$, where σ_ϑ denotes sigma of beam divergence. And finally, $\sigma_{\delta x} = P/\sqrt{12N}$.

Taking into account definitions (t, t_x and t_y are considered as positive here)

$$t = p^2\vartheta^2, \qquad t_x = t\cos^2\varphi, \qquad t_y = t\sin^2\varphi, \tag{A.5}$$

Eq. (A.4) can be rewritten in terms of t components:

$$t'_x = t\cos^2\varphi + p^2\delta^2\vartheta_x + \frac{p^2}{L_x^2}\delta x^2 + 2p\sqrt{t}\cos\varphi\left(\delta\vartheta_x + \frac{1}{L_x}\delta x\right). \tag{A.6}$$

The relation for t'_y can be obtained by swapping $x \leftrightarrow y$ and $\cos\varphi \leftrightarrow \sin\varphi$.

One can easily calculate mean value of t'_x while keeping t_x fixed (all terms linear in perturbations drop out because of their zero mean values):

$$\langle t'_x\rangle = t_x + p^2\left(\frac{\sigma_\vartheta^2}{4} + \frac{P^2}{12N\,L_x^2}\right). \tag{A.7}$$

Similarly, mean value of t' when t is fixed reads

$$\langle t'\rangle = t + p^2\left(\frac{\sigma_\vartheta^2}{2} + \frac{P^2}{12N\,L_x^2} + \frac{P^2}{12N\,L_y^2}\right). \tag{A.8}$$

In order to evaluate $\sigma_{t'_x}$, we need to calculate $\langle t'^2_x\rangle$. It is evident that terms linear in $\delta\vartheta_x$ and δx will not contribute. Also, to keep the calculation simple, terms higher than quadratic were not included.

$$t'^2_x = t_x^2 + 6p^2 t_x\left(\delta^2\vartheta_x + \frac{1}{L_x^2}\delta^2 x\right) + \ldots \tag{A.9}$$

And analogically

$$t'^2 = t^2 + 2p^2 t\left[(1+2\cos^2\varphi)\left(\delta^2\vartheta_x + \frac{1}{L_x^2}\delta^2 x\right) + (1+2\sin^2\varphi)\left(\delta^2\vartheta_y + \frac{1}{L_y^2}\delta^2 y\right)\right] + \ldots \tag{A.10}$$

[7] All the simulations in this note were performed using the smearing parameterization (7) in [2].

It is straight-forward to show that

$$\sigma^2_{t'_x} \equiv \left\langle t'^2_x \right\rangle - \left\langle t'_x \right\rangle^2 = 4p^2 t_x \left(\frac{\sigma^2_\vartheta}{4} + \frac{P^2}{12N\,L^2_x} \right) \qquad \text{for fixed } t_x \,, \tag{A.11}$$

$$\sigma^2_{t'} \equiv \left\langle t'^2 \right\rangle - \left\langle t' \right\rangle^2 = 4p^2 t \left[\frac{\sigma^2_\vartheta}{4} + \frac{P^2}{24N} \left(\frac{1}{L^2_x} + \frac{1}{L^2_y} \right) \right] \qquad \text{for fixed } t \,. \tag{A.12}$$

The relative resolution, then, gains the commonly used $A/\sqrt{t}$ form:

$$\frac{\sigma_{t'_x}}{t_x} = \frac{A}{\sqrt{t_x}}, \qquad A = 2p \sqrt{\frac{\sigma^2_\vartheta}{4} + \frac{P^2}{12N\,L^2_x}} \,, \tag{A.13}$$

$$\frac{\sigma_{t'}}{t} = \frac{A}{\sqrt{t}}, \qquad A = 2p \sqrt{\frac{\sigma^2_\vartheta}{4} + \frac{P^2}{24N} \left(\frac{1}{L^2_x} + \frac{1}{L^2_y} \right)} \tag{A.14}$$

Acknowledgements

I would like to express my gratitude to the team of TOTEM experiment, in particular to my advisors Mario Deile and Valentina Avati, for their support while writing this note.

References

[1] Barlow, R. J.: Statistics: a guide to the use of statistical methods in the physical sciences., *Wiley* (1989)

[2] Kašpar, J.: Description and simulation of beam smearing effects, *TOTEM-NOTE* **2007-005** (2007)